Matter

CellPress
OPEN ACCESS

Article

# Cathode-Electrolyte Interphase in Lithium Batteries Revealed by Cryogenic Electron Microscopy

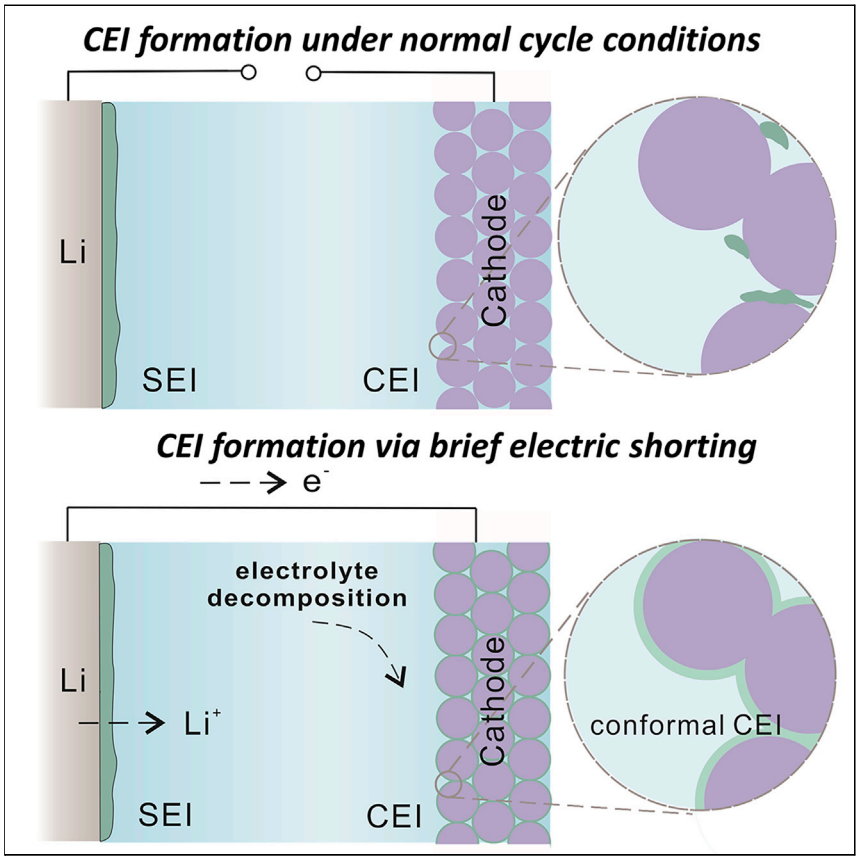


In contrast to its significance for battery performance, many aspects of the cathode-electrolyte interphase (CEI) remain elusive to the battery community. With cryogenic electron microscopy and spectroscopy, we find that there does not exist an intimate coating layer as a CEI in commercial carbonate-based electrolyte. However, upon brief external electrical shorting, a stable, conformal CEI can form *in situ* to help improve cycling stability.

Zewen Zhang, Jinlong Yang, William Huang, ..., Wenxiao Huang, Wah Chiu, Yi Cui

yicui@stanford.edu

HIGHLIGHTS

Cycled positive electrodes are preserved and characterized with cryo-EM

There is no intimate coating layer as CEI under normal cycling conditions

A stable conformal CEI can form *in situ* via brief electrical shorting

Cryo-(S)TEM and EELS reveals the chemistry of the conformal CEI

1 **Discovery**
A new material or phenomena

Zhang et al., Matter 4, 1–11
January 6, 2021 © 2020 The Authors. Published by Elsevier Inc.
https://doi.org/10.1016/j.matt.2020.10.021

Please cite this article in press as: Zhang et al., Cathode-Electrolyte Interphase in Lithium Batteries Revealed by Cryogenic Electron Microscopy, Matter (2020), https://doi.org/10.1016/j.matt.2020.10.021

Matter

CellPress
OPEN ACCESS

Article

# Cathode-Electrolyte Interphase in Lithium Batteries Revealed by Cryogenic Electron Microscopy

Zewen Zhang,[1,8] Jinlong Yang,[1,2,3,8] William Huang,[1] Hansen Wang,[1] Weijiang Zhou,[4] Yanbin Li,[1] Yuzhang Li,[1] Jinwei Xu,[1] Wenxiao Huang,[1] Wah Chiu,[4,5,6] and Yi Cui[1,7,9,*]

## SUMMARY

**Cathode electrolyte interphase (CEI), the intimate coating layer formed on the positive electrode, has been thought to be critical. However, many aspects of CEI remain unclear. This originates from the lack of effective tools to characterize structural and chemical properties of these sensitive interphases at nanoscale. Here, we develop a protocol to preserve the native state and directly visualize the interface on the positive electrode using cryogenic electron microscopy. We find that under normal operation conditions, there does not exist an intimate coating layer at the single-particle level in carbonate-based electrolyte. However, upon brief external electrical shorting, a solid-electrolyte interphase, which usually forms on anodes, could form on cathodes and be electrochemically converted into a stable, conformal CEI *in situ*. The conformal CEI helps improve Coulombic efficiency and overall capacity retention of the battery. This generates a different perspective of CEI in commercial carbonate-based electrolytes than previously understood.**

## INTRODUCTION

Lithium-ion batteries, the state-of-the-art secondary battery technology, have revolutionized modern energy storage. Due to the extreme operating potentials of both the positive and negative electrodes, new solid phases, with an electrolyte nature, form at the electrode-electrolyte interface via electrochemical decomposition of the electrolytes. These so-called solid-electrolyte interphases (SEI) influence the insertion of $Li^+$ from the solvated phase into the solid phase and constitute the rate-limiting step for lithiation of most electrode materials.[1] Given the importance of these interphases to the battery performance, there has been extensive characterization of them in different systems using various methods.[2–5]

However, unlike the negative electrode (anode) SEI, the SEI on the positive electrode (cathode), or cathode-electrolyte interphase (CEI), has been less thoroughly studied. This is in part because the operating potentials of most positive electrodes do not deviate much from the thermodynamic stability window of the commercial carbonate electrolytes.[6] Meanwhile, the rich surface chemistry on the positive electrode side involving alkyl carbonate electrolytes, including acid-base reactions, nucleophilic reactions, induced polymerizations, and transition metal dissolution, introduce extra complexity to CEI studies.[7]

Notably, the scope of CEI definition varies in the literature. Besides the intimate coating layer from electrolyte decomposition, the cathode surface reconstruction layer and dynamic adsorption layer of soluble species have also been included as

### Progress and Potential

Fundamental understanding of the electrode-electrolyte interface is key to the improvement of state-of-the-art batteries and the design of emerging batteries. The cathode-electrolyte interphase (CEI) remains unclear in many aspects. Using cryogenic electron microscopy, we preserve the native state and visualize the interface on positive electrodes. Contrary to common belief, we discovered that there does not exist an intimate coating layer of CEI at the single-particle level in carbonate-based electrolytes. However, upon brief electrical shorting, a solid-electrolyte interphase could form on cathodes and be electrochemically turned into a stable, conformal CEI *in situ* to improve battery performance. Our results provide a new perspective on CEI, inspire a powerful tool to engineer CEI in different electrolyte systems with various additives, and highlight the importance of correlating microscopic nanostructure and macroscopic chemical information when studying these sensitive interphases.


This is an open access article under the CC BY-NC-ND license (http://creativecommons.org/licenses/by-nc-nd/4.0/).

a CEI.[8,9] To avoid confusion, we define CEI here as the intimate coating layer with the nature of solid-electrolyte on the positive electrode, which corresponds to its original definition as the SEI on the positive electrode.[10,11]

The CEI species are believed to resemble those of SEI.[7] However, controversies still exist among reports from different research groups regarding its morphology, functionality, and even its existence as a protective film.[12,13] These ambiguities likely exist due to the simultaneous lack of both structural and chemical information. On one hand, characterization techniques such as X-ray photoelectron spectroscopy (XPS),[14] neutron reflectometry,[15] nuclear magnetic resonance,[16] and surface enhanced Raman spectroscopy[8] that could probe the chemistry of these interphase species are limited in in-plane spatial resolution due to the ensemble signals they collect. On the other hand, techniques such as atomic force spectroscopy,[17] which produce high spatial resolution, lack chemical information.

The nanoscale morphology, complex chemical nature, reactivity to air and moisture,[18] and sensitivity to X-ray and electron beam radiation[19] have made characterization of the CEI difficult. Even after obtaining structural information and chemical information with high spatial resolution at the same time, other factors might affect the interpretation of such observations. For example, soluble SEI species from the anode side,[20] trapped electrolyte residue in highly porous electrode, or unintentional brief shorting during battery assembly or disassembly (Figure S1) could not be differentiated from CEI species.

Therefore, it is of vital importance to directly visualize the structure and reveal the function of this complex interphase at the atomic scale. Recent advances in cryogenic transmission electron microscopy (cryo-TEM) has enabled atomic-resolution imaging and high-resolution chemical characterization of air-sensitive and beam-sensitive battery materials, especially SEI on Li metal anodes,[21–24] carbonaceous anodes,[25] and silicon anodes.[26] Considering the similarity in chemical nature of CEI and SEI and the reactivity of these sensitive battery materials, cryogenic electron microscopy (cryo-EM) offers new opportunities to investigate CEI.

## RESULTS AND DISCUSSION

### Lack of Intimate CEI Layer under Normal Cycle Conditions

To prevent possible artifacts in CEI introduced during sample preparation, we took special care in experimental design. First, we synthesized nanoparticles of positive electrode materials as model systems (Figures 1E, S2A, and S2B) to avoid conventional TEM sample preparation such as microtomy or focused-ion beam, which may introduce chemical or mechanical artifacts. Nanoparticles provide a sharp view of the interface, and the high surface-to-volume ratio presumably results in more significant CEI growth to facilitate electrochemical CEI characterization. Second, at the electrode level, we used a relatively low loading of active materials ($\sim$2 mg cm$^{-2}$) to ensure cycling of all electrode materials and reduce possible electrolyte residue trapped during sample preparation. Third, we used minimum solvent to gently rinse the whole electrode after cycling and scraped the electrode with a clean fine tweezer tip to load nanoparticles onto TEM grids to avoid other possible mechanical artifacts that might have arisen had sonication been used. Fourth, we adopted cryo-transfer procedures to avoid exposure to air or other possible side reactions, Figure 1A illustrates the main sample preparation and transfer procedures, whereby the entire sample preparation and transfer procedure is either in argon or liquid $N_2$ environment; for details see Experimental Procedures.

[1]Department of Materials Science and Engineering, Stanford University, Stanford, CA 94305, USA

[2]College of Materials Science and Engineering, Shenzhen University, Shenzhen 518060, China

[3]School of Advanced Materials, Peking University, Shenzhen Graduate School, Shenzhen 518055, China

[4]Biophysics Program, School of Medicine, Stanford University, Stanford, CA 94305, USA

[5]Department of Bioengineering, Stanford University, Stanford, CA 94305, USA

[6]Division of CryoEM and Bioimaging, SSRL, SLAC National Accelerator Laboratory, Menlo Park, CA 94025, USA

[7]Stanford Institute for Materials and Energy Sciences, SLAC National Accelerator Laboratory, 2575 Sand Hill Road, Menlo Park, CA 94025, USA

[8]These authors contributed equally

[9]Lead Contact

*Correspondence: yicui@stanford.edu

https://doi.org/10.1016/j.matt.2020.10.021

Please cite this article in press as: Zhang et al., Cathode-Electrolyte Interphase in Lithium Batteries Revealed by Cryogenic Electron Microscopy, Matter (2020), https://doi.org/10.1016/j.matt.2020.10.021



CellPress
OPEN ACCESS

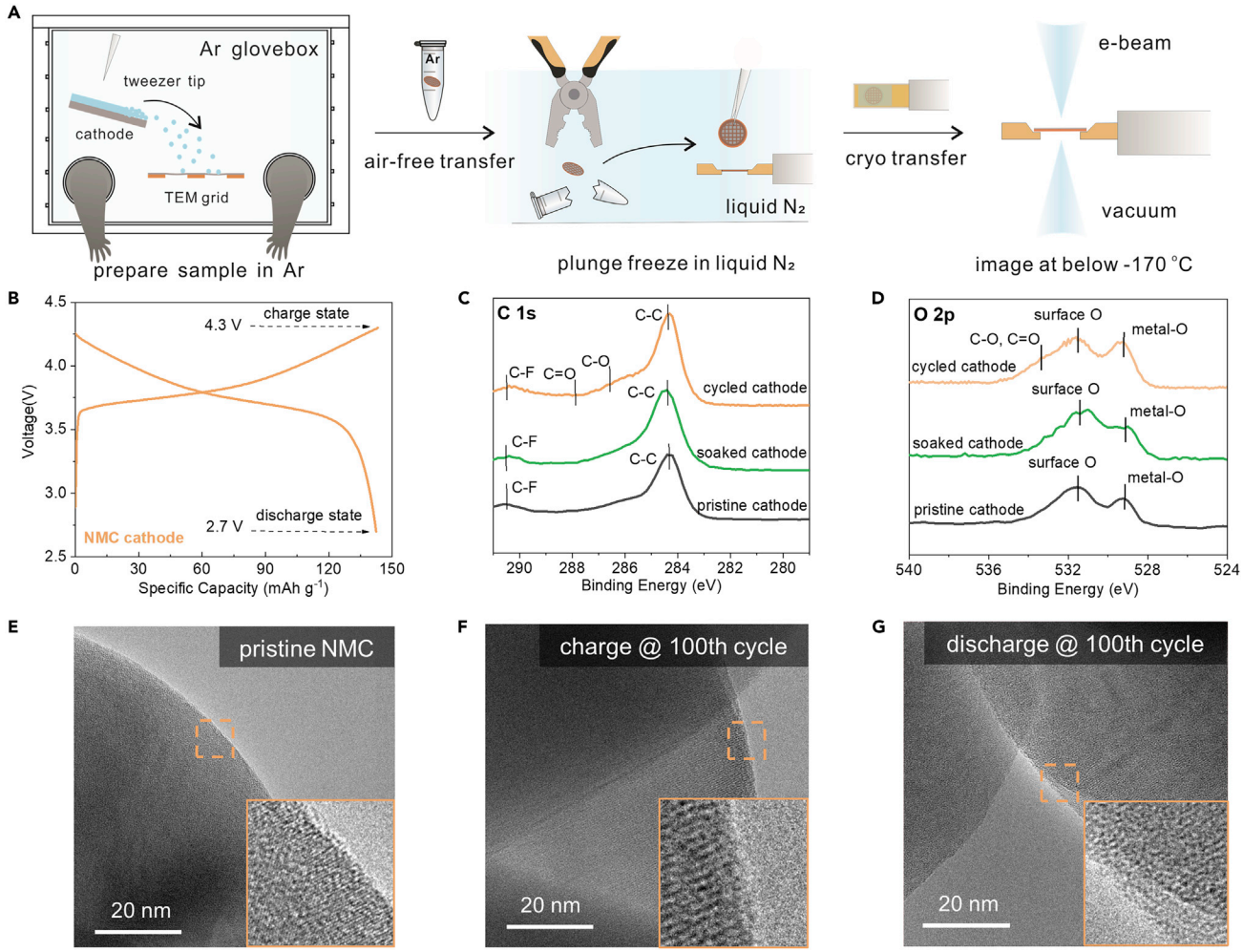


**Figure 1. Sample Preparation Schemes for Cryo-EM, and Cryo-EM Images for Cycled Positive Electrode**

(A) The entire process of sample preparation and transfer for cryo-EM is either in argon or liquid $N_2$ to avoid air exposure or other possible side reactions.

(B) The charge-discharge profile of as-synthesized NMC nanoparticle electrode shows typical electrochemical behavior of NMC electrodes.

(C and D) Carbon 1s (C) and oxygen 2p (D) XPS spectra of pristine and cycled NMC electrode.

(E–G) High-resolution cryo-EM images of pristine (E) and cycled (charged, F, and discharged, G state) NMC electrode surfaces show no apparent formation of coating layer.

See also Figures S3–S6.

Air-free XPS indicates the existence of CEI species on the cycled electrode (cycled between 2.7 and 4.3 V), although we did not find a well-defined CEI layer under cryo-EM on the same sample. Compared with pristine lithium nickel manganese cobalt oxide (NMC) sample and NMC soaked in electrolyte for 24 h, cycled NMC samples show C–O peaks in C 1s spectra (Figure 1C) as well as in O 2p spectra (Figure 1D) in XPS, suggesting the formation of CEI species, consistent with XPS results in previous reports.[14,27] However, for deep cycled NMC electrodes shown in Figures 1C and 1G, the morphology of the surface of both charge- and discharge-state electrodes also do not deviate much from the pristine electrode, without any film attached to the particles. This suggests that the as-claimed CEI is not an intimate coating layer on the electrode.

Since a wider consensus in the battery community is that sustained electrolyte decomposition would happen at higher voltage, we also worked with lithium- and

Please cite this article in press as: Zhang et al., Cathode-Electrolyte Interphase in Lithium Batteries Revealed by Cryogenic Electron Microscopy, Matter (2020), https://doi.org/10.1016/j.matt.2020.10.021



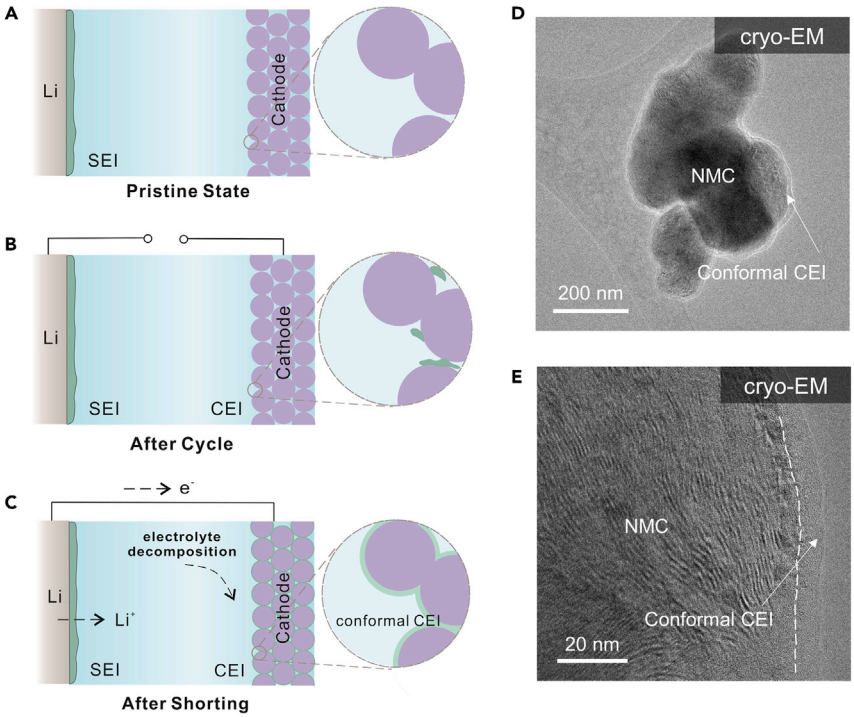


**Figure 2. Schematics for CEI Formation under Different Conditions, and Cryo-EM Characterization of Conformal CEI**

(A–C) Schematics for positive electrodes in different states: pristine cathodes (A), CEI formed during normal cycling conditions (B), and conformal CEI formed via electrical shorting mechanism (C).

(D and E) Cryo-EM images of conformal CEI formed on NMC-positive electrodes.

See also Figures S15 and S16.

manganese-rich (LMR) NMC positive electrodes. We find that the lack of an intimate coating layer is also the case for these electrodes cycled to both 4.6 V and 4.8 V (Figure S9) but note that LMR particles showed a more rugged surface after prolonged cycles (Figure S9), which indicates a more active electrode-electrolyte interaction at the interface. It has been proposed that sustained oxidation of interphase species and gas evolution (CO, $CO_2$) might occur at this high voltage.[28–30] This helps explain why a well-defined CEI layer is absent at the particle interface despite the fact that widely expected intense oxidation reactions are also happening. This has been observed for multiple samples under all of these conditions (Figures S7–S14).

For all conditions of cycled electrodes described above, we did not observe a clear interphase layer on the positive electrode particle, as occurs on most negative electrodes. This is either because CEI is highly heterogeneously distributed on the positive electrode and does not cover each individual particle uniformly as a coating layer, or because the amount of CEI species are limited even with prolonged cycling in the electrolyte and do not precipitate out as solid interphases. These results indicate that though commonly believed to share similar chemical compositions as SEI on negative electrodes, CEI does have a vastly different distribution and morphology on the electrode (Figure 2B). This might also be in accordance with reported adsorption behavior of soluble species, whereby CEI species experience adsorption and desorption on the electrode during cycling. However, it is also important to point out that in other electrolyte systems, such as ether-based

Please cite this article in press as: Zhang et al., Cathode-Electrolyte Interphase in Lithium Batteries Revealed by Cryogenic Electron Microscopy, Matter (2020), https://doi.org/10.1016/j.matt.2020.10.021





electrolytes[22] or electrolytes with additives that are capable of film formation, there still could be formation of intimate coating layer.[31–33]

### *In Situ* Generated Conformal CEI Layer via Electrochemical Shorting

Based on the observation of the absence of intimate coating on electrodes under cryo-EM and the fact that reported CEI has chemistry nature similar to that of SEI, we introduce a facile way to form a stable conformal CEI *in situ* by learning from the mechanism of SEI formation at anodes. It is generally accepted that a stable and uniform CEI is critical in preventing parasitic side reactions at the interface, such as sustained electrolyte oxidation and acid etching of electrode materials.[29] By shorting the assembled cell briefly (for about 20 s), we can quickly bring down the potential on the positive electrode to beyond the stability window of electrolytes. Subsequent electrolyte decomposition would occur to form an SEI-like coating on the positive electrode (Figure 2C), and this intimate SEI coating layer would turn into CEI in the subsequent cycling. It is important to point out that the shorting reaction needs to be very brief so that the electrolyte readily decomposes to form a conformal layer on cathodes before introducing structural and/or chemical damage to the electrodes. It is highly possible a kinetically controlled reduction process whereby electrolyte decomposition is much faster than further electrode reduction. The chemical pathways for the CEI generated should be similar to that for SEI formation on the anode side.

Under cryo-EM, we observe a conformal thin layer of CEI after brief shorting on the positive electrode particle (Figures 2D, 2E, S15, and S16). The electrode particle is uniformly coated with a thin layer of mostly amorphous materials spanning ~5–10 nm at the edge of the interface. The moiré pattern here may indicate a slight overlithiation of the surface layer during the shorting, which is also reflected in the first charge curve in Figure S24. After the first cycle, the charge-discharge profile becomes normal. After cycling back to cathode potential for few cycles, this coating layer remains intact (Figure S17). We also observed a similar thin, primarily amorphous layer on conductive carbon additives (Figure S18). This suggests that the formation of CEI is uniform throughout the electrode. The fact that it is generally thinner on the carbon black seems to indicate a catalytic effect of cathode surface chemistry on CEI formation.

### Structural and Chemical Characterization of Conformal CEI

In addition to structural information through high-resolution TEM, we also obtained chemical information from cryogenic scanning TEM electron energy loss spectroscopy (cryo-STEM EELS). Cryo-STEM EELS mapping of a region containing the electrode, conformal CEI, and carbon black additives yields an annular dark-field image (Figure S20) along with a C K-edge map, O K-edge map, and Mn L-edge map as shown in Figure 3A. Corresponding mapping of a pristine positive electrode is shown in Figure S21. The C K-edge map shows a uniform carbon distribution throughout the coating layer. In the O K-edge map, compared with the Mn L-edge map the larger region with high intensity confirms the existence of significant oxygen within this conformal CEI layer. The C K-edge EELS fine structure (Figure 3A) is dominated by the peaks at around 288 eV and 290 eV, indicating C–H bonding and carbonate bonding, respectively. The entire C K-edge and O K-edge of both conformal region and carbon black region are shown in Figure S22. The bonding environment and amorphous structure of this conformal CEI suggests the organic polymeric composition of alkyl carbonates. Air-free XPS results with ensemble signals from larger sample areas support the same conclusion. C 1s and O 2p spectra of conformal CEI show significantly increased C=O and C–O signals as compared with pristine electrodes (Figures 3C and 3D). We also

Please cite this article in press as: Zhang et al., Cathode-Electrolyte Interphase in Lithium Batteries Revealed by Cryogenic Electron Microscopy, Matter (2020), https://doi.org/10.1016/j.matt.2020.10.021



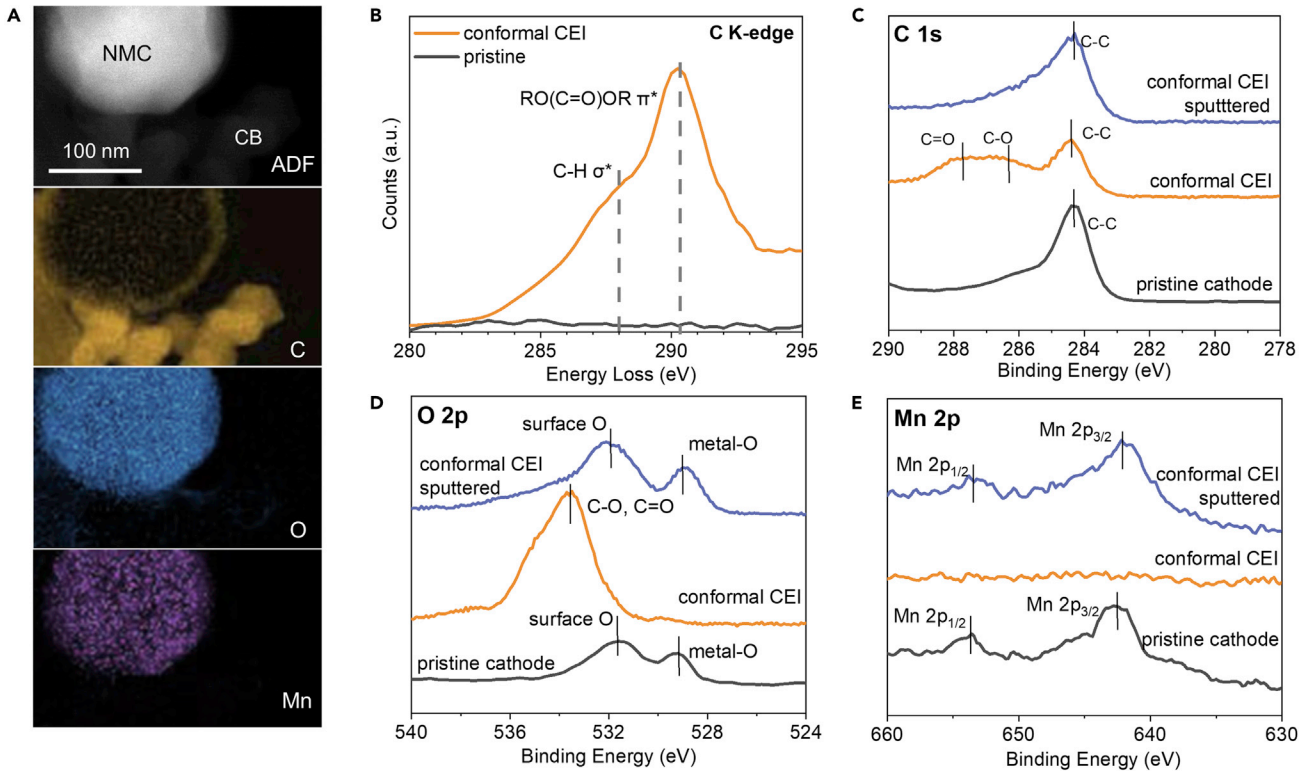


**Figure 3. Chemical and Electrochemical Analysis of Conformal CEI**

(A) Annular dark-field image and cryo-STEM EELS mapping of conformal CEI on NMC electrodes (yellow, carbon element; blue, oxygen element; purple, manganese element).

(B) EELS fine structure of carbon K-edge in pristine positive electrode and conformal CEI.

(C–E) XPS spectra of pristine, cycled NMC electrode, and electrode with conformal CEI carbon 1s spectrum (C), oxygen 2p spectrum (D), and manganese 2p spectrum (E).

do not see a fluorine peak in the spectrum, which means that LiF is not a component in the CEI (Figure S23). It is very interesting that Mn 2p spectra here show barely any Mn signal (Figure 3E). The absence of Mn signal also indicates that there is little transition metal loss during the CEI formation and the as-formed CEI is uniformly coated over the whole electrode.

## Impact of Conformal CEI on Positive Electrode Performance

This conformal CEI interface on the electrode effectively segregates active species from the electrolyte while allowing $Li^+$ transport, and side reactions from electrode-electrolyte reactions are largely suppressed. At a moderate rate of 0.5 C, an NMC-positive electrode with a conformal CEI was able to deliver a cycling specific capacity of $\approx$147 mAh $g^{-1}$ (based on NMC mass), which could be attributed to nanosized particles where a better rate capability is expected. NMC with conformal CEI also exhibits a smaller and slower increase in overpotential during charge and discharge as shown in Figure S24. Electrochemical impedance spectroscopy results also suggested the same conclusion (Figure 4B). This could be attributed to a better-maintained and stable interface against electrolyte, where side reactions such as acid etching from the electrolyte are suppressed. Notably, the average Coulombic efficiency of the initial ten cycles (without the first charge cycle) is improved from around 91% to 98% (Figure 4A). This effect could also be observed under other shorting conditions (Figures S25 and S26; Table S1). The overall capacity retention of electrodes with a conformal CEI layer is also enhanced. With a conformal CEI, a

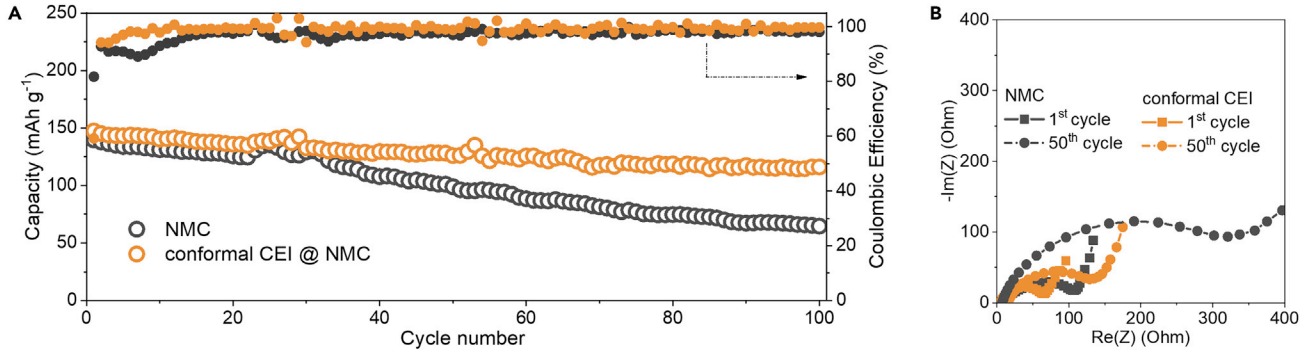


**Figure 4. Electrochemical Analysis of Conformal CEI**

(A) Long cycle performance of pristine NMC electrodes and NMC electrodes with conformal CEI at a rate of C/2.

(B) Electrochemical impedance spectroscopy of both pristine electrodes and electrodes with conformal CEI at 1st and 50th cycle (black, pristine electrodes; orange, positive electrodes with conformal CEI).

discharge capacity of 116 mAh $g^{-1}$ at the 100th cycle could be achieved, while pristine electrode only maintained a specific capacity of 64 mAh $g^{-1}$ at this cycle. Note that compared with microsized positive electrodes a faster capacity decay is expected here, since higher surface-to-volume ratio of nanosized positive electrode particles will lead to a more significant interfacial effect.

## Conclusions

We investigate the interface on the positive electrode in standard carbonate electrolyte at atomic scale with cryo-EM and reveal that an intimate coating layer does not exist on the positive electrode. However, we also found that upon brief external electrical shorting between anodes and cathodes, an SEI, which usually forms at the anode surface, could form on cathodes and be electrochemically converted into a stable, conformal CEI *in situ*. The conformal CEI provides uniform passivation to the positive electrode while maintaining the ionic transport pathway, which suppresses undesirable side reactions between electrode and electrolyte. As a result, a higher Coulombic efficiency and capacity retention could be achieved in the positive electrode. The conformal CEI formation mechanism provides a powerful tool to broaden the scope of interfacial chemistries design on positive electrodes. SEI design principles and recipes can now be applied to CEI engineering.

In a broader context, direct imaging and characterization of this sensitive interphase preserved in native state at atomic scale provides a new dimension in the metric table to investigate the interfacial chemistries between electrodes and electrolytes, which is essential in understanding electrode evolution and battery-failure mechanisms. This is applicable to a variety of cathode chemistry and electrolyte combinations beyond conventional intercalation-type cathodes in carbonates, such as conversion-type sulfur cathode in ether-based electrolytes,[34] conversion-type metal fluoride cathode in carbonate-based electrolytes,[35] and intercalation-type NMC cathode in high-concentration ether-based electrolytes.[36] Therefore, new insights from various systems highlighted by this method would help make possible the rational design of electrodes and electrolytes for emerging battery chemistry.

## EXPERIMENTAL PROCEDURES

### Resource Availability

#### *Lead Contact*

Further information and request for resources and reagents should be directed to and will be fulfilled by the Lead Contact, Yi Cui (yicui@stanford.edu).

*Materials Availability*

This study did not generate new unique reagents.

*Data and Code Availability*

This study did not generate/analyze datasets or code.

## Materials Synthesis

For the NMC532-positive electrode, 0.152 mol of lithium acetate dihydrate ($LiCH_3COO{\cdot}2H_2O$, Sigma-Aldrich), 0.75 mol of nickel acetate tetrahydrate ($Ni(CH_3COO)_2{\cdot}4H_2O$, Sigma-Aldrich), 0.45 mol of manganese acetate tetrahydrate ($Mn(CH_3COO)_2{\cdot}4H_2O$, Sigma-Aldrich), and 0.03 mol of cobalt acetate tetrahydrate ($Co(CH_3COO)_2{\cdot}4H_2O$, Sigma-Aldrich) were dissolved in 150 mL of distilled water; 0.23 mol of oxalic acid ($H_2C_2O_4{\cdot}2H_2O$, Sigma-Aldrich) was dissolved in 750 mL of ethanol. The mixed water solution was quickly poured into the ethanol solution and kept at room temperature under stirring for 12 h. Precursor was obtained through solvent evaporation. The synthesized precipitates were then calcined at 450°C for 8 h and at 850°C for 20 h in air with a ramping rate of 2.0°C $min^{-1}$ to obtain $LiNi_{0.5}Co_{0.2}Mn_{0.3}O_2$-positive electrode materials. The LMR cathode materials were synthesized from the above procedure but using a ratio of Li/Mn/Ni/Co = 1.2:0.56:0.16:0.08.

## Electrochemical Measurements

Working electrodes were all prepared using a conventional slurry method. Positive electrode nanoparticles, carbon black conductive additive (TIMCAL Super P), and polyvinylidene fluoride (Kynar HSV 900) binder with a mass ratio of 8:1:1 was dispersed in *N*-methyl-2-pyrrolidone. After stirring overnight, the slurry was cast onto a carbon-coated Al foil with doctor blade and dried at 60°C in a vacuum oven for 12 h, after which the samples were calendared and cut into 1-$cm^2$ circular disks with a mass loading of ~2.0 mg $cm^{-1}$. In an argon-filled glovebox, these electrodes were assembled into type 2032 coin cells with a polymer separator (Celgard 2325) and Li metal (Alfa Aesar) as the counter/reference electrode. Sixty microliters of carbonate-based electrolyte with 1 M lithium hexafluorophosphate in 1:1 (v/v) ethylene carbonate/diethyl carbonate (BASF Selectilyte LP40) was added as the electrolyte for full wetting of both working and counter electrode surfaces. Coin cells were loaded into a battery tester (Land Instruments) and cycled between 2.5 V and 4.3 V at a C-rate of C/2. Charge/discharge rates were calculated assuming the theoretical capacity of positive electrode materials (1C = 150 mAh $g^{-1}$ for NMC 532, = 250 mAh $g^{-1}$ for LMR).

## External Electrical Shorting Experiment

We formed SEI on cathodes by external electrical shorting. After assembly, coin cells were rested at OCV (open-circuit voltage) for 1 h and then clamped by a pair of conducting metal tweezers to become shorted for different period lengths, including 1 s, 10 s, 20 s, 30 s, and >120 s. In the main text, the conformal CEI samples were shorted for 20 s while the overly shorted samples were shorted for more than 120 s.

## Materials Characterization

SEM images were taken using an FEI Magellan 400 XHR scanning electron microscope with an acceleration voltage of 5 kV and a probe current of 25 pA. The XPS spectra were collected using a PHI VersaProbe Scanning XPS Microprobe with an Al (Kα) source. The sputtering process helps remove the material layer by layer on the characterized surface.

Please cite this article in press as: Zhang et al., Cathode-Electrolyte Interphase in Lithium Batteries Revealed by Cryogenic Electron Microscopy, Matter (2020), https://doi.org/10.1016/j.matt.2020.10.021





### TEM Sample Preparation and Cryo-Transfer

The batteries were disassembled in an argon-filled glovebox and rinsed with pure diethyl carbonate to remove Li salts. Our rinsing procedure attempts to minimize artifacts by using minimal force and solvent volume; in total approximately 300 μL was carefully dropped onto the whole electrode after the battery was disassembled, each time with 100 μL. Immediately after rinsing, we used a clean fine tweezer tip to gently scrape the electrode to obtain positive electrode nanoparticles on the TEM grids. The TEM sample was then sealed in an airtight container, which was quickly submerged in liquid nitrogen and crushed in liquid nitrogen to rapidly expose the sample to cryogen without air exposure. While immersed in liquid nitrogen, the sample was loaded into the cryo-EM holder (Gatan626) and inserted into the TEM column. The cryo-EM holder uses a specialized shutter to prevent air exposure and ice condensation onto the sample, which preserves the specimen in its native state. Once inside the TEM column, the temperature was maintained at approximately −178°C.

### Transmission Electron Microscopy

Cryo-EM experiments were performed on a Thermo Fisher Titan Krios G2 transmission electron microscope operated at 300 kV and equipped with an autoloading mechanism. Cryo-EM images were acquired by a Gatan K3 direct-detection camera in the electron-counting mode. Several short-exposure (0.1 s) single-frame shots were taken to estimate the defocus and make it as close as possible to Scherzer defocus. Cryo-EM images were taken with an electron dose rate of around 60 $e^{-}/Å^{2}/s$, and a total of 10 frames were taken with 0.1 s per frame for each image. Dose fraction frames were motion-corrected by MotionCor2 to correct beam-induced movements. Conventional and cryo-(S)TEM characterizations were carried out using an FEI Titan 80-300 environmental (scanning) transmission electron microscope operated at an accelerating voltage of 300 kV with an energy resolution of 1 eV. The instrument is equipped with an aberration corrector in the image-forming lens, which was tuned before each sample analysis. Conventional TEM images were taken with a dose rate of over 1,000 $e^{-}/Å^{2}/s$, and an exposure time for each image of around 0.1 s with built-in drift correction function in GMS3. Cryo-STEM EELS characterization was performed with a C2 aperture of 50 mm, a beam current of 10 pA, a camera length of 77 mm, and a pixel dwell time of 100 ms. EELS spectra were acquired on a GIF Quantum 966 with a dispersion of 0.25 eV/channel in Dual EELS mode, with the low-loss centered on the zero-loss peak and the core-loss centered on the C K-edge. Energy drift during spectrum imaging was corrected by centering the zero-loss peak to 0 eV at each pixel. Maps were computed through a two-window method, with a pre-edge window fitted to a power-law background and a post-edge window of 20–40 eV on the core-loss signal.

## SUPPLEMENTAL INFORMATION

Supplemental Information can be found online at https://doi.org/10.1016/j.matt.2020.10.021.

## ACKNOWLEDGMENTS

Y.C. and W.C. acknowledge the cryo-EM research support from the Department of Energy, Office of Basic Energy Sciences, Division of Materials Science and Engineering under contract DE-AC02-76SF00515. Yuzhang Li acknowledges the Intelligence Community Fellowship for funding. Z.Z. acknowledges support from Stanford Interdisciplinary Graduate Fellowship. We acknowledge the use and support of the Stanford-SLAC CryoEM Facilities. Part of this work was performed at the Stanford Nano

Shared Facilities (SNSF), supported by the National Science Foundation under award ECCS-2026822.

## AUTHOR CONTRIBUTIONS

Z.Z. and J.Y. contributed equally to this work. Z.Z. and Y.C. conceived the project and design the experiments. J.Y. performed materials synthesis. J.Y. and Z.Z. performed electrochemical measurements. Z.Z. and W.Z. carried out cryo-EM experiments. W.Z. processed the CTF-corrected images. H.W., W.H., W.Z., Yuzhang Li, and Yanbin Li helped with the characterizations. Z.Z., J.Y., and Y.C. co-wrote the manuscript. All authors discussed the results and commented on the manuscript.

## DECLARATION OF INTERESTS

The authors declare no competing interests.

Received: July 15, 2020
Revised: September 14, 2020
Accepted: October 15, 2020
Published: November 9, 2020

## REFERENCES

1. Peled, E., and Menkin, S. (2017). Review—SEI: past, present and future. J. Electrochem. Soc. *164*, A1703–A1719.

2. Peled, E. (1979). The electrochemical behavior of alkali and alkaline earth metals in nonaqueous battery systems—the solid electrolyte interphase model. J. Electrochem. Soc. *126*, 2047–2051.

3. Arora, P., White, R.E., and Doyle, M. (1998). Capacity fade mechanisms and side reactions in lithium-ion batteries. J. Electrochem. Soc. *145*, 3647–3667.

4. Aurbach, D. (2000). Review of selected electrode-solution interactions which determine the performance of Li and Li ion batteries. J. Power Sources *89*, 206–218.

5. Pinson, M.B., and Bazant, M.Z. (2013). Theory of SEI formation in rechargeable batteries: capacity fade, accelerated aging and lifetime prediction. J. Electrochem. Soc. *160*, A243–A250.

6. Xu, K. (2014). Electrolytes and interphases in Li-ion batteries and beyond. Chem. Rev. *114*, 11503–11618.

7. Aurbach, D., Markovsky, B., Salitra, G., Markevich, E., Talyossef, Y., Koltypin, M., Nazar, L., Ellis, B., and Kovacheva, D. (2007). Review on electrode-electrolyte solution interactions, related to cathode materials for Li-ion batteries. J. Power Sources *165*, 491–499.

8. Chen, D., Mahmoud, M.A., Wang, J.-H., Waller, G.H., Zhao, B., Qu, C., El-Sayed, M.A., and Liu, M. (2019). Operando investigation into dynamic evolution of cathode-electrolyte interfaces in a Li-ion battery. Nano Lett. *19*, 2037–2043.

9. Yang, P., Zheng, J., Kuppan, S., Li, Q., Lv, D., Xiao, J., Chen, G., Zhang, J.-G., and Wang, C.-M. (2015). Phosphorus enrichment as a new composition in the solid electrolyte interphase of high-voltage cathodes and its effects on battery cycling. Chem. Mater. *27*, 7447–7451.

10. Wrodnigg, G.H., Besenhard, J.O., and Winter, M. (1999). Ethylene sulfite as electrolyte additive for lithium-ion cells with graphitic anodes. J. Electrochem. Soc. *146*, 470–472.

11. Strauss, E., Golodnitsky, D., and Peled, E. (1998). Cathode modification for improved performance of rechargeable lithium/composite polymer electrolyte-pyrite battery. Electrochem. Solid State Lett. *2*, 115–117.

12. Dupré, N., Martin, J.-F., Oliveri, J., Soudan, P., Guyomard, D., Yamada, A., and Kanno, R. (2009). Aging of the $LiNi_{1/2}Mn_{1/2}O_2$ positive electrode interface in electrolyte. J. Electrochem. Soc. *156*, C180–C185.

13. Würsig, A., Buqa, H., Holzapfel, M., Krumeich, F., and Novák, P. (2005). Film formation at positive electrodes in lithium-ion batteries. Electrochem. Solid State Lett. *8*, A34–A37.

14. Zhang, J.-N., Li, Q., Wang, Y., Zheng, J., Yu, X., and Li, H. (2018). Dynamic evolution of cathode electrolyte interphase (CEI) on high voltage $LiCoO_2$ cathode and its interaction with Li anode. Energy Storage Mater. *14*, 1–7.

15. Minato, T., Kawaura, H., Hirayama, M., Taminato, S., Suzuki, K., Yamada, N.L., Sugaya, H., Yamamoto, K., Nakanishi, K., Orikasa, Y., et al. (2016). Dynamic behavior at the interface between lithium cobalt oxide and an organic electrolyte monitored by neutron reflectivity measurements. J. Phys. Chem. C *120*, 20082–20088.

16. Cuisinier, M., Dupré, N., Martin, J.-F., Kanno, R., and Guyomard, D. (2013). Evolution of the $LiFePO_4$ positive electrode interface along cycling monitored by MAS NMR. J. Power Sources *224*, 50–58.

17. Lu, W., Zhang, J., Xu, J., Wu, X., and Chen, L. (2017). In situ visualized cathode electrolyte interphase on $LiCoO_2$ in high voltage cycling. ACS Appl. Mater. Interfaces *9*, 19313–19318.

18. Schroder, K.W., Celio, H., Webb, L.J., and Stevenson, K.J. (2012). Examining solid electrolyte interphase formation on crystalline silicon electrodes: influence of electrochemical preparation and ambient exposure conditions. J. Phys. Chem. C *116*, 19737–19747.

19. Lin, F., Markus, I.M., Doeff, M.M., and Xin, H.L. (2014). Chemical and structural stability of lithium-ion battery electrode materials under electron beam. Sci. Rep. *4*, 5694.

20. Fang, S., Jackson, D., Dreibelbis, M.L., Kuech, T.F., and Hamers, R.J. (2018). Anode-originated SEI migration contributes to formation of cathode-electrolyte interphase layer. J. Power Sources *373*, 184–192.

21. Li, Y., Li, Y., Pei, A., Yan, K., Sun, Y., Wu, C.-L., Joubert, L.-M., Chin, R., Koh, A.L., Yu, Y., et al. (2017). Atomic structure of sensitive battery materials and interfaces revealed by cryo-electron microscopy. Science *358*, 506–510.

22. Wang, X., Zhang, M., Alvarado, J., Wang, S., Sina, M., Lu, B., Bouwer, J., Xu, W., Xiao, J., Zhang, J.-G., et al. (2017). New insights on the structure of electrochemically deposited lithium metal and its solid electrolyte interphases via cryogenic TEM. Nano Lett. *17*, 7606–7612.

23. Zachman, M.J., Tu, Z., Choudhury, S., Archer, L.A., and Kourkoutis, L.F. (2018). Cryo-STEM mapping of solid-liquid interfaces and dendrites in lithium-metal batteries. Nature *560*, 345–349.

24. Li, Y., Huang, W., Li, Y., Pei, A., Boyle, D.T., and Cui, Y. (2018). Correlating structure and function of battery interphases at atomic resolution using cryoelectron microscopy. Joule *2*, 2167–2177.

25. Huang, W., Attia, P.M., Wang, H., Renfrew, S.E., Jin, N., Das, S., Zhang, Z., Boyle, D.T., Li, Y.,

Please cite this article in press as: Zhang et al., Cathode-Electrolyte Interphase in Lithium Batteries Revealed by Cryogenic Electron Microscopy, Matter (2020), https://doi.org/10.1016/j.matt.2020.10.021



Bazant, M.Z., et al. (2019). Evolution of the solid-electrolyte interphase on carbonaceous anodes visualized by atomic-resolution cryogenic electron microscopy. Nano Lett. *19*, 5140–5148.

26. Huang, W., Wang, J., Braun, M.R., Zhang, Z., Li, Y., Boyle, D.T., McIntyre, P.C., and Cui, Y. (2019). Dynamic structure and chemistry of the silicon solid-electrolyte interphase visualized by cryogenic electron microscopy. Matter *1*, 1232–1245.

27. Li, Q., Wang, Y., Wang, X., Sun, X., Zhang, J.-N., Yu, X., and Li, H. (2020). Investigations on the fundamental process of cathode electrolyte interphase formation and evolution of high-voltage cathodes. ACS Appl. Mater. Interfaces *12*, 2319–2326.

28. Jung, R., Metzger, M., Maglia, F., Stinner, C., and Gasteiger, H.A. (2017). Chemical versus electrochemical electrolyte oxidation on NMC111, NMC622, NMC811, LNMO, and conductive carbon. J. Phys. Chem. Lett. *8*, 4820–4825.

29. Dedryvère, R., Foix, D., Franger, S., Patoux, S., Daniel, L., and Gonbeau, D. (2010). Electrode/electrolyte interface reactivity in high-voltage spinel $LiMn_{1.6}Ni_{0.4}O_4/Li_4Ti_5O_{12}$ lithium-ion battery. J. Phys. Chem. C *114*, 10999–11008.

30. Duncan, H., Abu-Lebdeh, Y., and Davidson, I.J. (2010). Study of the cathode-electrolyte interface of $LiMn_{1.5}Ni_{0.5}O_4$ synthesized by a sol-gel method for Li-ion batteries. J. Electrochem. Soc. *157*, A528–A535.

31. Jiao, S., Ren, X., Cao, R., Engelhard, M.H., Liu, Y., Hu, D., Mei, D., Zheng, J., Zhao, W., Li, Q., et al. (2018). Stable cycling of high-voltage lithium metal batteries in ether electrolytes. Nat. Energy *3*, 739–746.

32. Li, J., Li, W., You, Y., and Manthiram, A. (2018). Extending the service life of high-Ni layered oxides by tuning the electrode-electrolyte interphase. Adv. Energy Mater. *8*, 1801957.

33. Cabana, J., Kwon, B.J., and Hu, L. (2018). Mechanisms of degradation and strategies for the stabilization of cathode-electrolyte interfaces in Li-ion batteries. Acc. Chem. Res. *51*, 299–308.

34. Wei Seh, Z., Li, W., Cha, J.J., Zheng, G., Yang, Y., McDowell, M.T., Hsu, P.-C., and Cui, Y. (2013). Sulphur-$TiO_2$ yolk-shell nanoarchitecture with internal void space for long-cycle lithium-sulphur batteries. Nat. Commun. *4*, 1331.

35. Wang, F., Robert, R., Chernova, N.A., Pereira, N., Omenya, F., Badway, F., Hua, X., Ruotolo, M., Zhang, R., Wu, L., et al. (2011). Conversion reaction mechanisms in lithium ion batteries: study of the binary metal fluoride electrodes. J. Am. Chem. Soc. *133*, 18828–18836.

36. Ren, X., Zou, L., Jiao, S., Mei, D., Engelhard, M.H., Li, Q., Lee, H., Niu, C., Adams, B.D., Wang, C., et al. (2019). High-concentration ether electrolytes for stable high-voltage lithium metal batteries. ACS Energy Lett. *4*, 896–902.